

12-12-91
E-6064

NASA Technical Memorandum 103787

Spatial Variations in A.C. Susceptibility and Microstructure for the $\text{YBa}_2\text{Cu}_3\text{O}_{7-x}$ Superconductor and Their Correlation with Room-Temperature Ultrasonic Measurements

Don J. Roth
Lewis Research Center
Cleveland, Ohio

Mark R. DeGuire
Case Western Reserve University
Cleveland, Ohio

Leonard E. Dolhert
W.R. Grace & Company
Columbia, Maryland

and

Aloysius F. Hepp
Lewis Research Center
Cleveland, Ohio

Prepared for the
93rd Annual Meeting of the American Ceramic Society
Cincinnati, Ohio, April 28-May 2, 1991

NASA

SPATIAL VARIATIONS IN A.C. SUSCEPTIBILITY AND MICROSTRUCTURE FOR THE
 $\text{YBa}_2\text{Cu}_3\text{O}_{7-x}$ SUPERCONDUCTOR AND THEIR CORRELATION WITH ROOM-TEMPERATURE
ULTRASONIC MEASUREMENTS

Don J. Roth
National Aeronautics and Space Administration
Lewis Research Center
Cleveland, Ohio 44135

Mark R. DeGuire
Department Materials Science and Engineering
Case Western Reserve University
Cleveland, Ohio 44106

Leonard E. Dolhert
W.R. Grace and Company
Research Division
Columbia, Maryland 21044

and

Aloysius F. Hepp
National Aeronautics and Space Administration
Lewis Research Center
Cleveland, Ohio 44135

ABSTRACT

The purpose of this study was to (1) examine the spatial (within-sample) uniformity of superconducting behavior and microstructure in $\text{YBa}_2\text{Cu}_3\text{O}_{7-x}$ specimens over the pore fraction range 0.10 to 0.25 and (2) determine the viability of using a room-temperature, nondestructive characterization method (ultrasonic velocity imaging) to predict spatial variability. Spatial variations in a.c. susceptibility were observed for specimens containing 0.10 pore fraction. An ultrasonic velocity image constructed from measurements at 1 mm increments across one such specimen revealed microstructural variation between edge and center locations that correlated with variations in a.c. shielding and loss behavior. Optical quantitative image analysis on sample cross sections revealed pore fraction to be the varying microstructural feature.

INTRODUCTION

The last several years have seen the remarkable development of a new class of ceramics exhibiting superconductivity to unprecedentedly high temperatures (refs. 1 to 4). The subject of this study is the $\text{YBa}_2\text{Cu}_3\text{O}_{7-x}$ (YBCO) superconductor. Microstructural and compositional variations have been shown to result in significant electrical and magnetic property variations in (YBCO) (refs. 5 to 8). Based on previous observations concerning ceramics, (refs. 9 and 10) it is possible that such microstructural and property variations are present within individual YBCO parts. Knowledge and minimization of such spatial variation is a critical requirement both to quantitative analysis (predictability) of the superconductor's behavior and to attempts to optimize properties such as normal-to-superconducting transition temperature

and critical current density (refs. 11 and 12).

In this study, spatial variations in microstructure and properties were investigated for YBCO specimens over the pore fraction range 0.10 to 0.25. The study was comprised of two experiments. In the first experiment, a.c. susceptibility measurements were used to examine superconducting behavior at edge and center locations of specimens without having prior knowledge of microstructural/compositional differences at these locations. In the second experiment, an ultrasonic scan technique was employed to locate within-sample microstructural nonuniformity in a YBCO disk. Susceptibility measurements subsequently were made at the locations indicated to be nonuniform from ultrasonic images. Microstructural analysis was performed on several sample sections to determine the microstructural feature(s) responsible for the variability observed in ultrasonic images.

EXPERIMENTAL

Specimens

Five YBCO disk-shaped samples (labeled 1 to 4 and A) were manufactured. YBCO powder for the samples was made by first dissolving the appropriate amount of metal nitrates in water, and then coprecipitating a hydroxy-carbonate by mixing aqueous tetramethylammonium carbonate with the aqueous nitrate solution. The precipitate was then filtered and dried. The dried solids were precalcined in air at 540 °C for 5 hr to remove organic matter, and then calcined in flowing air at 880 °C for 50 hr followed by cooling to 300 °C over 16 hr. At 600 °C, flowing air was shut off and replaced by flowing oxygen. Two batches of starting powder were made, one for samples 1 to 4 and one for sample A.

The synthesized YBCO powder was ball-milled for 1.5 hr in a polyurethane-lined jar mill with highly wearresistant yttria-stabilized zirconia balls. The powder and balls were separated by shaking them in a stainless steel 100-mesh sieve. Jar loading and unloading, and sieving were done in a low-CO₂/low-H₂O glovebox. This procedure produced a powder with a broad size distribution. Average particle size was about 1.5 μm with no particles greater than 45 μm.

Disks approximately 25.4 mm diameter by 6.3 mm thick were made by die-pressing at 3000 to 5000 psi followed by cold isostatic-pressing at 20000 psi for 5 min. The sample disks, sitting on 20-mesh MgO single crystals, were sintered and cooled according to the schedule of table I in a 7 cm diameter tube furnace with flowing, ultra-high purity oxygen (flow rate = 200 to 240 cm³/min). (Sample 1 experienced an

Table I. - HEATING/SINTERING/COOLING SCHEDULE FOR YBCO SAMPLES

Segment	Heat to: temperature, °C	Cool to: temperature, °C	For: time, hrs.	Atmos- phere
1	100	---	0.167	Oxygen ↓
2	Peak	---	4.5	
3	Peak hold	---	1.5	
4	-----	600	2	
5	-----	300	13	
6	-----	200	1	
7	-----	25	9	

argon cooling before subsequently being reheated in argon and cooled in oxygen, essentially mimicking the oxygenation of the other samples.)

The peak sintering temperature for sample disks 1 to 4 was altered to obtain a range of pore fractions. Samples 1 to 4 had peak sintering temperatures of 937, 947, 954, and 966 °C (±2 °C), resulting in pore fractions of 0.25, 0.22, 0.21 and 0.10 (±0.005), respectively. (Pore fraction was

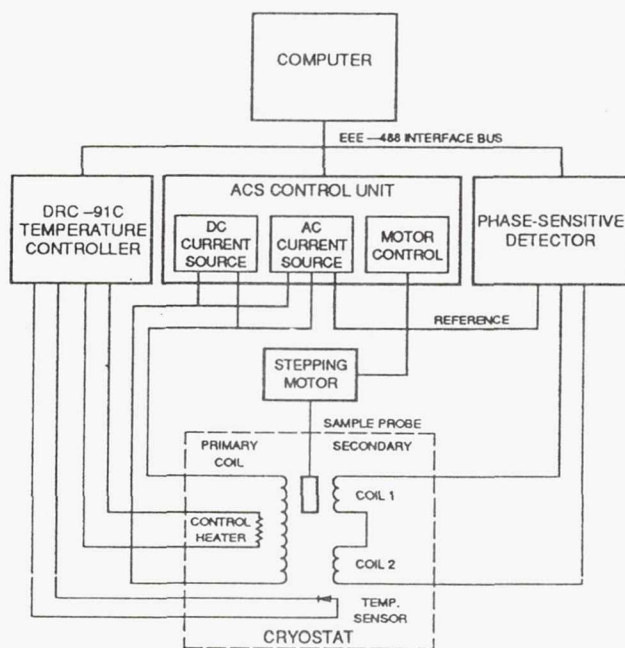
determined from sample mass and dimensions, and assuming a bulk density of 6.38 g/cm^3 for fully-dense YBCO.) Samples 1 to 4 were dry cut into two thinner disks 3 mm thick using a slitting saw with a 180 grit diamond-impregnated steel blade. A bar of approximate dimensions 10 mm by 3 mm by 2 mm was then dry cut from the edge and center regions of one of the disks from samples 1 to 4. In preparation for a.c. susceptibility measurements, the bars were dry machined flat and parallel to a 0.025 mm tolerance on a surface grinder using a 150 grit diamond wheel.

Sample disk A had a peak sintering temperature of 942°C and contained 0.10 (+ 0.005) pore fraction. (Sample A had as low a pore fraction as did sample 4 even though it was peak sintered at a much lower peak temperature (942°C versus 966°C). This may have indicated a difference in impurity content between the batches of starting powders from which samples 1 to 4 and sample A were made.) Sample A was machined flat and parallel to $2.678 \pm 0.002 \text{ mm}$ in preparation for ultrasonic scanning. After scanning, bars (approximately 5 by 3 by 2 mm) were cut from edge and center locations for susceptibility measurements.

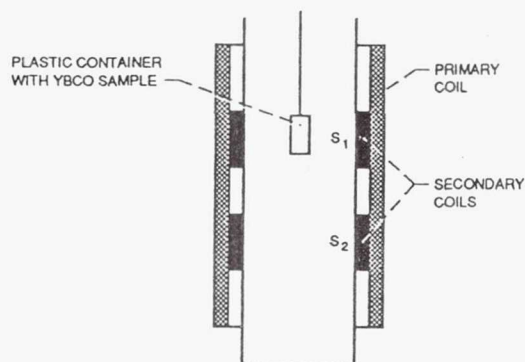
All samples were handled with gloves to minimize contamination and were stored in a desiccator when not in experimentation to avoid atmospheric attack.

A.C. Susceptibility

(See appendix A for information concerning the use of a.c. susceptibility for measuring superconductor properties.) The complex a.c. susceptibility (χ) was used to measure a.c. flux exclusion (shielding) and loss for the edge- and center-cut bars from samples 1 to 4, and A using the Lakeshore Cryotronics (Westerville, OH 43081) Model 7000 susceptometer (fig. 1). The measuring principle is



(a) Schematic of susceptometer.



(b) Cross-sectional view of the sample/coil assembly.

Figure 1 - Instrumentation and set-up for a.c. susceptibility measurements.

as follows (ref. 13). An alternating magnetic field is applied to the sample by means of an alternating current through a primary coil. A system of two secondary coils oppositely wound and connected in series is used to detect the variation in magnetic flux created by the sample when it is located in one of the secondary coils. The coil assembly resides inside of a cryostat and is surrounded by shielding material to minimize the influence of the Earth's magnetic field. The resulting signal is measured by a phasesensitive detector which produces a complex output voltage proportional

to the complex susceptibility of the sample. The output voltage and thus the susceptibility are separated into real (χ') (in-phase) and imaginary (χ'') (out-of-phase) parts.

The bars were lightly ground to remove possible contaminants and then ultrasonically cleaned in fresh ethanol (and air-dried) before measurements. Each bar was placed into a small non-magnetic plastic sample container. The container with specimen was attached to a nonmagnetic plastic rod which was connected to a stepping motor. The specimens were cooled to 4.2 K in zero field, the field was applied (parallel to the specimen long axis), and the assembly was heated to 100 K through the superconducting-to-normal (S-N) transition at a rate of 0.7 K/min. The applied a.c. field (H_{ac}) and frequency (f) were 0.020 Oe and 100 Hz, respectively. No d.c. field was applied. Approximately one null measurement (ref. 8) per degree Kelvin was obtained by precisely and automatically moving the container between the centers of the two secondary (sensing) coils (fig. 1(b)) and obtaining data at the center of each coil.

Mass susceptibilities were obtained from (ref. 14)

$$\chi_m = \frac{\chi}{\rho} \quad (1)$$

where χ_m is the mass susceptibility and ρ is the bulk density of the sample. The susceptibilities were external, i.e. demagnetization corrections were not made. (The demagnetization factor is estimated at 0.05 for rectangular bars of the dimensions used in this study (ref. 14)). Susceptibility was calculated taking sample volume to be the bulk volume (material + pores) of the sample. The uncertainty in the absolute susceptibility measurement was estimated at 4 percent for samples 1 to 4 and 10 percent for sample A (due to the uncertainties in the bar dimensions and the accuracy

with which voltage is read by the phase sensitive detector). The uncertainty in the absolute temperature measurement was conservatively estimated at 0.5 K.

The following properties were derived from susceptibility measurements: percent of maximum shielding at 77 K (%MS(77K)), the superconducting transition temperature (T_c), the transition width (ΔT_{cm}), and the loss peak width. Percent MS(77K) was defined as

$$\%MS(77K) = \left[\frac{\chi'_m(77K)}{\chi'_m(4.2K)} \right] \cdot 100 \quad (2)$$

where $\chi'(77K)$ and $\chi'(4.2K)$ are the shielding at 77 K and 4.2 K, respectively. (Maximum shielding is defined as the value of χ' obtained at 4.2 K.) T_c was determined from the onset temperature of the normal-to-superconducting (N-S) transition in χ' . ΔT_{cm} was determined from the difference in temperatures for which 10 and 90 percent of maximum shielding were achieved during the N-S transition. Loss peak width was obtained from the difference in temperature between the initial rise from and return to zero in χ'' .

Ultrasonics

(See appendix B for information concerning the use of ultrasonic velocity for revealing material differences.) Longitudinal wave velocity measurements were obtained at room temperature over an ordered array of points across the surface for sample A by means of an auto-mated scanning technique (fig. 2), (refs. 8 and 15). The pulse echo contact technique (fig. 3) was used to obtain ultrasonic waveform data (refs. 16 and 17). In this technique, an ultrasonic pulse generated by a piezoelectric crystal is propagated into a buffer rod-couplant-sample (BCS) configuration. The ultrasound reflects off the front and back surfaces of the sample and travels back

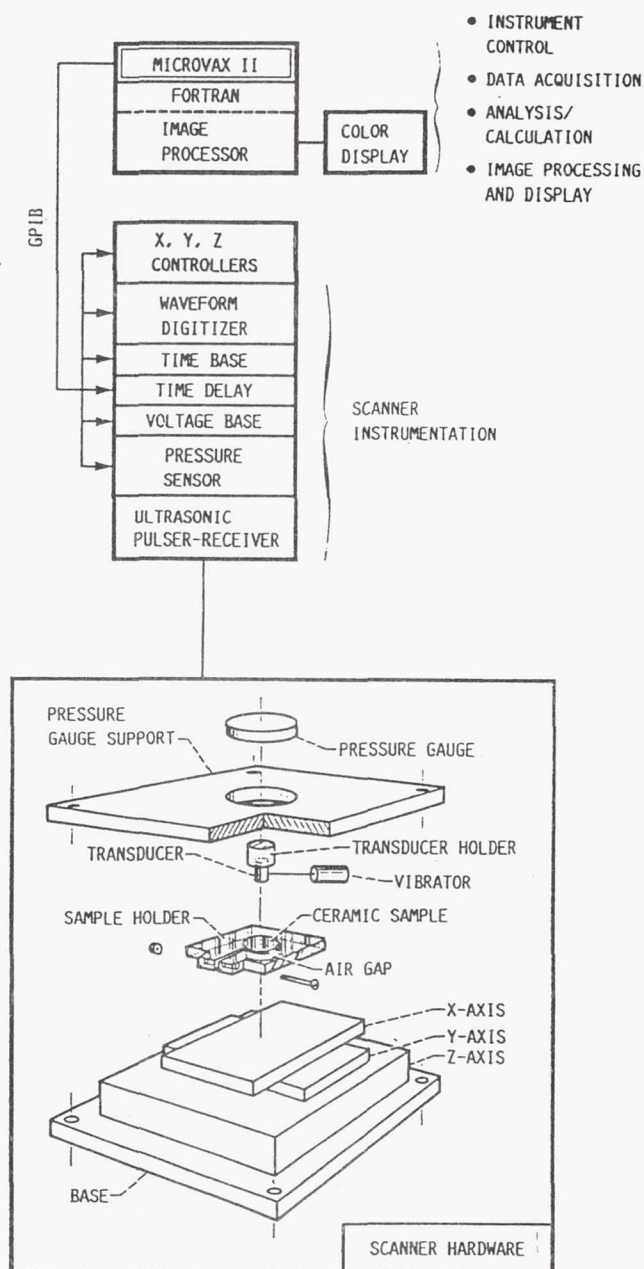
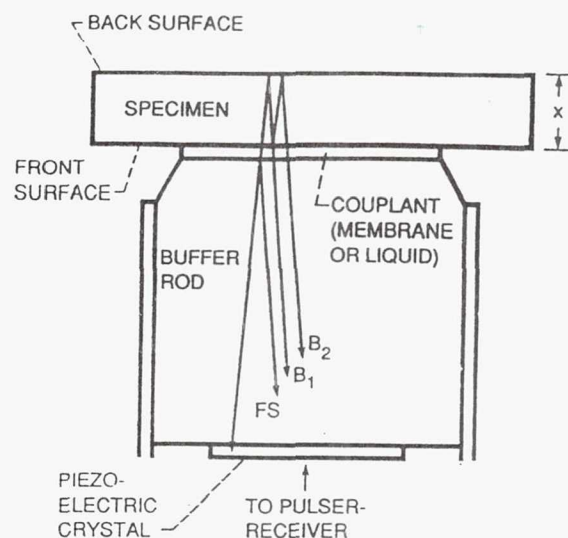
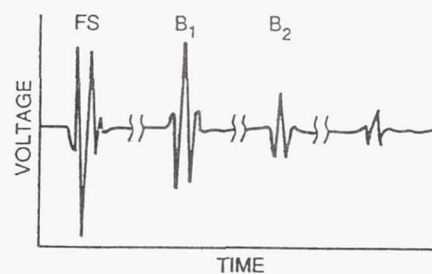


Figure 2. - Computer-controlled acoustic scanning system.

to the crystal. The ultrasonic transducer (Panametrics, Waltham, MA 02254) used was a broadband 20-MHz (center frequency) type having a lead metaniobate crystal with an active diameter of 6 mm. The crystal was bonded to a silica glass buffer rod approximately 17.5 mm in diameter and 12.7 mm in length. A pulser-receiver having a 1 to 150 MHz bandwidth was used to electrically pulse the crystal



(a) Diagram of transducer/specimen configuration for pulse-echo ultrasonics.



(b) Resulting waveforms.

FS \equiv Front surface reflection
 B_1 \equiv first back surface reflection
 B_2 \equiv second back surface reflection

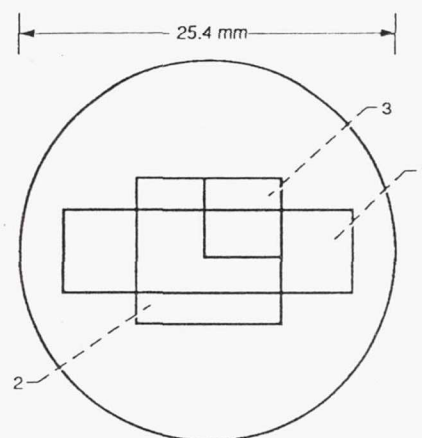
Figure 3. - Pulse-echo contact technique.

and receive the pulses reflected from the sample. The pulses were digitized into 512 point arrays at a sampling rate of 1.024 GHz. Each pulse was acquired 64 times and averaged to reduce noise levels. The time delay between the back-surface-reflected pulses B_1 and B_2 (fig. 3), and the sample thickness (x), were used to calculate cross-correlation velocity (ref. 17). Velocity determined from cross-correlation is essentially a group velocity as the entire wave train (containing a broad band of frequencies) is considered in the calculation.

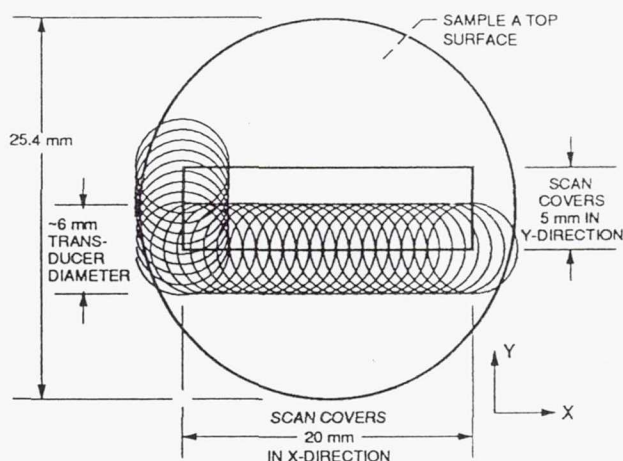
In preparation for scanning, sample A was mounted in a Lucite holder.

A nonaqueous liquid couplant (Dow Corning [Midland, MI 48640] 704 diffusion pump fluid) was used between the transducer buffer rod and sample to allow ultrasonic transmission. The contact force on the transducer was maintained at 12 ± 0.1 lbs. After a set of waveforms was acquired at one point, the x- and or y- positioner table was automatically moved the specified increment to the next point. A vibrator (made from a modified electric scribing tool) was used during this movement to aid in repositioning of transducer and couplant, and to prevent the transducer from jamming on the sample.

Three areas of sample A were scanned as shown in figure 4(a). Scan 1 was over a 20 by 5 mm rectangular area (area 1) with measurements made every 1 mm. Scan 2 was over a 10 by 10 mm square area (area 2) overlapping area 1 with measurements made every 1 mm. Scan 3 was over a 6 by 6 mm square area (area 3) that fit into the upper right hand corner of area 2 with measurements made every 0.5 mm. If one considers the volume element probed by the beam, ultrasonic data were actually obtained over a larger region by about 6 mm for each of the x and y dimensions (fig. 4(b)). (The volume element probed is determined by the ultrasonic beam diameter, ultrasonic wave-length and sample thickness (refs. 18 and 19). For our experimental configuration, significant beam spreading is not likely to occur as the beam does not extend into the far field. Thus, the (0 to -20 dB) beam width can be estimated by the active transducer diameter (ref. 18)). Typical scan and analysis times for scans consisting of 100 to 150 measurements were about 1 to 2 hr. Scans were run at least twice for each specimen region examined to determine reproducibility. It was estimated that the uncertainty in the velocity measurement for sample A was ≤ 0.36 percent with the major sources of error being specimen and couplant thickness variation, and thickness measurement inaccuracy.



(a) Top view of sample A showing regions that were ultrasonically scanned.



(b) Schematic of ultrasonic scan for region 1 of sample A. 20 mm (x-direction) by 5 mm (y-direction) scan with 1-mm transducer increments. Transducer positions shown for $x = 1 - 21$, $y = 0$, and $x = 0$, $y = 1 - 6$. In total, there are 21 transducer positions along x-axis and 6 transducer positions along y-axis to give 126 measurements in scan.

Figure 4 - Ultrasonic scans for sample A.

An ultrasonic image was constructed from the velocity values obtained at each scan point. A continuous scale consisting of 256 shades of gray (or color) and linear interpolation between points allowed the display of subtle velocity changes across the sample (ref. 15). The image can be thought of as a two-dimensional projection representing averaged microstructural information for the volume of sample scanned.

MICROSTRUCTURAL AND COMPOSITIONAL ANALYSIS

All Samples

The edge- and center-cut bars of samples 1 to 4 and A were examined for microstructural and compositional differences. Bright field optical microscopy with polarized light was used to obtain grain and porosity distribution micrographs. Mean grain size was obtained from the optical micrographs using the Heyn-intercept method (ASTM E112-85). Grain size was determined for four orientations of the micrograph. Estimated uncertainty in mean grain size was about 20 percent.

X-ray diffraction was performed on top and bottom surfaces of the bars with a computer-controlled diffractometer using $\text{CuK}(\alpha)$ radiation. In several instances, material was ground from the surfaces and the sample rescanned to determine whether compositional deviations were present within the bulk. A least-squares refinement procedure was used to determine the unit cell axis lengths. The starting powders for the two batches used to make samples 1 to 4 and sample A were examined for impurities with x-ray diffraction.

The number of oxygen atoms per YBCO molecule was determined for the bars from the c-axis length using an empirical relationship

$$\frac{\text{atoms}_{\text{oxygen}}}{\text{molecule}_{\text{YBCO}}} = 76.40 - 5.95 (\text{c-axis})^{(3)}$$

for which the estimated uncertainty was 0.05 atoms oxygen (ref. 20). Weight percent oxygen was determined for the bars from inert gas fusion for which the estimated uncertainty was about 1 percent of the reading.

General analysis on the YBCO samples included the following. Concentrations of Y, Ba, and Cu were

accomplished with inductively-coupled plasma atomic emission spectroscopy (ICP-AES) for which the estimated uncertainty was about 3 to 5 percent of the determination. Colorimetric analysis was used to determine the concentration of any Si impurity with estimated uncertainty about 10 percent of the reading. Scanning electron microscopy (SEM) in both the back-scatter and secondary electron modes was used to examine polished and fracture surfaces of YBCO samples for topography and possible contamination. Energy dispersive (EDS) and wavelength dispersive (WDS) x-ray spectroscopy were used for elemental analysis of foreign structures. Transmission electron microscopy (TEM) in conjunction with electron diffraction and EDS was used to identify the presence of CuO in thin sections of YBCO.

Optical Image Analysis for Sample A

Upon completion of ultrasonic scanning, sample A was cut into two semicircular halves in preparation for microstructural analysis (fig. 5). A computer-controlled image analysis system was employed to quantify the average sizes (length and breadth) and volume fractions of pores and CuO grains. One half of sample A was mounted and polished on an automatic polisher to expose the cross section of the disk (fig. 5(b)). At each of 5 locations from left to right across the diameter, 21 fields in a straight line downward through the entire thickness were analyzed and the resulting sizes and areal fractions averaged. Averaging these values through the sample thickness mimicks the ultrasonic measurement. The cross section was examined two more times after removing 1.1 mm and then 6 mm of material (fig. 5(b)). For the first two cuts of the cross section, five left to right locations separated by 5 mm were examined. For the last examination, three

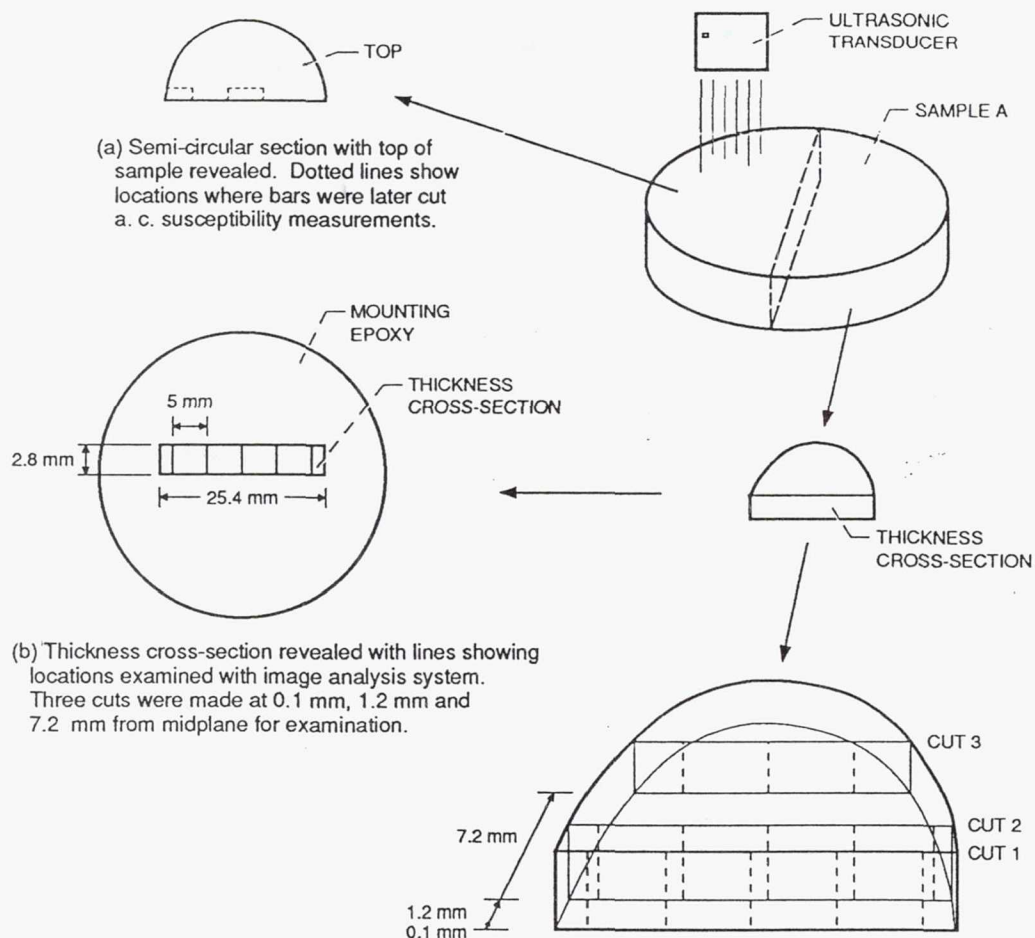


Figure 5. - Sections cut from sample A for optical examination.

locations separated by 5 mm were examined since the disk was substantially reduced in size. The analyzer was operated in the semi-automatic mode with manual readjustment of gray level and focus at each measurement field. Estimated uncertainties in the size and volume fraction measurements from repeated trials was on the order of 10 percent.

RESULTS

Samples 1 to 4

Figures 6(a) to (d) show percent of maximum shielding at 77 K (%MS(77K)), transition temperature (T_c), magnetic transition width (ΔT_{cm}), and the temperature width of the loss peak,

respectively, versus pore fraction for the edge- and center-cut bars of samples 1 to 4. The values of these superconductor properties were very similar at edge and center locations except for sample 4 containing 0.10 pore fraction. Figure 7 shows the a.c. susceptibility versus temperature responses and table II gives the superconductor properties for the edge- and center-cut bars of sample 4. For sample 4, the center-cut bar exhibited a T_c of 90 K and a broad ΔT_{cm} of 12 K. The edge-cut bar exhibited a lower T_c of about 82 K and a sharper ΔT_{cm} of about 4 K. Percent MS(77K) was about 1.5 times as large for the center-cut bar as for the edge-cut bar. The loss peak width was about twice as great for the center-cut bar as for the edge-cut bar.

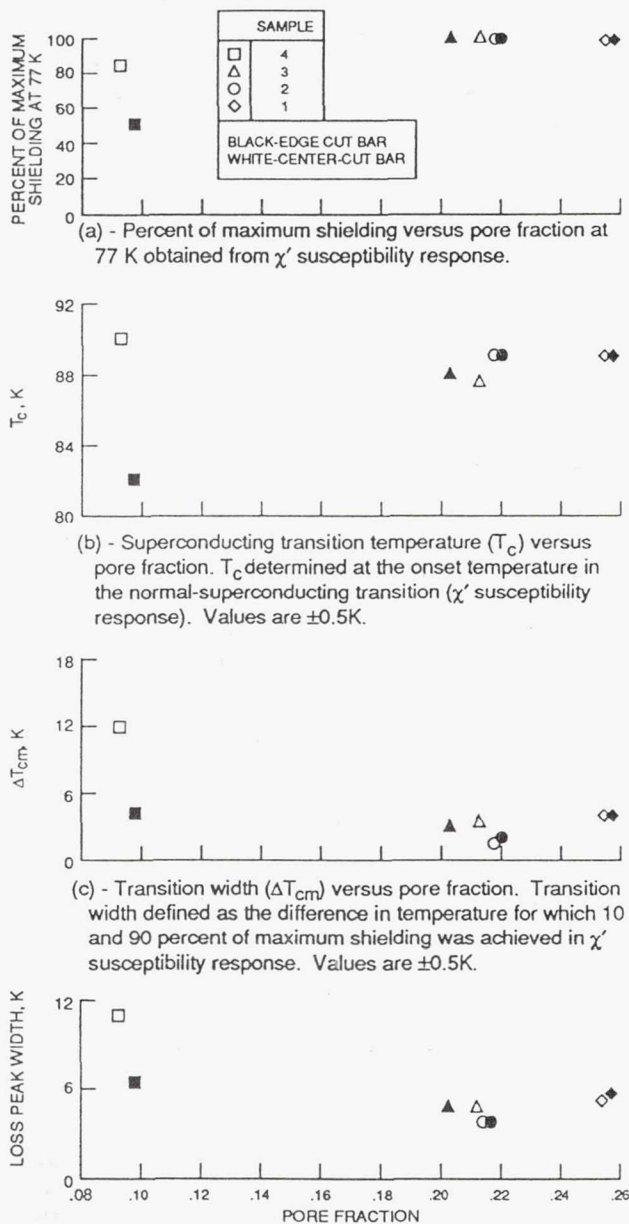


Figure 6. - Superconductor behavior of bars cut from samples 1, 2, 3, and 4.

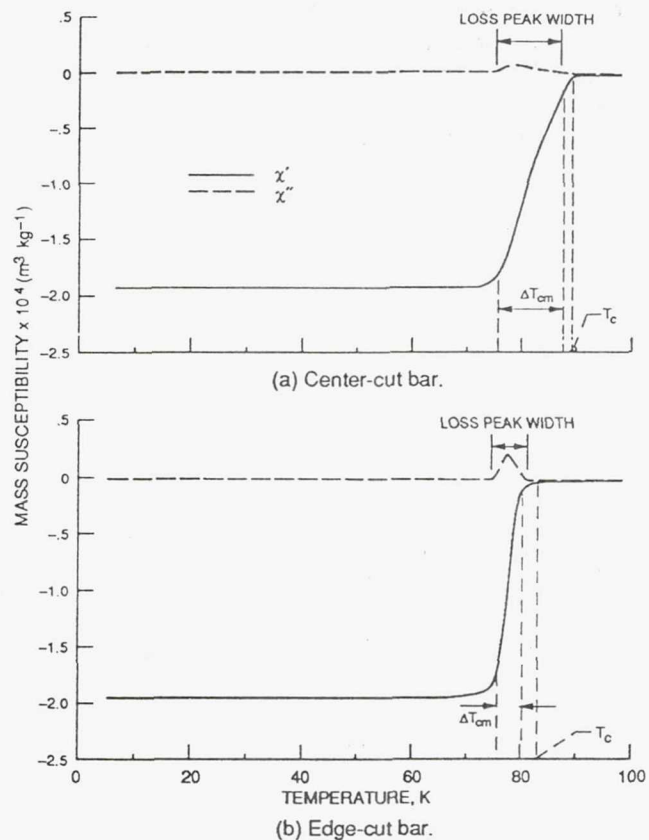


Figure 7. - A.c. susceptibility versus temperature for bars cut from sample 4. $H_{ac} = 0.02 \text{ Oe}$. Frequency = 100 Hz.

Table II. - SUPERCONDUCTOR BEHAVIOR FOR CENTER- AND EDGE-CUT BARS OF SAMPLES 4 AND A

Property	Sample 4		Sample A	
	Center-cut bar	Edge-cut bar	Center-cut bar	Edge-cut bar
Percent of maximum shielding at 77 K ^a	84	50	0	40
T_c (K)	90 \pm 0.5	82 \pm 0.5	75 \pm 0.5	86 \pm 0.5
ΔT_{cm} (K)	12 \pm 0.5	4 \pm 0.5	4 \pm 0.5	16.5 \pm 0.5
Width of loss peak(s) (K)	11 \pm 1	6.5 \pm 1	7 \pm 1	4.5, 9 \pm 1

^aSee equation (2).

The differing susceptibility responses for the edge- and center-cut bars of sample 4 indicated possible microstructural and/or compositional inhomogeneity (ref. 7). The possibility of oxygen inhomogeneity in the sample was likely since T_c is so critically dependent on oxygen content (ref. 6). Table III summarizes the

microstructural and compositional characteristics of the edge- and center-cut bars for sample 4. No significant differences were noted in either the unit cell parameters, grain size or oxygen content for the edge- and center-cut bars of sample 4. Samples 1 to 3 were uniform in composition and microstructure from analyses as well.

Table III. - MICROSTRUCTURAL AND COMPOSITIONAL CHARACTERISTICS FOR
CENTER- AND EDGE-CUT BARS FROM SAMPLES 4 AND A

Property	Sample 4		Sample A	
	Center-cut bar	Edge-cut bar	Center-cut bar	Edge-cut bar
Bar dimensions (cm):				
Length	1.0003±0.0005	0.9990±0.0005	0.51±0.03	0.50±0.03
Width	0.2995±0.0005	0.2999±0.0005	0.310±0.001	0.304±0.001
Height	0.2495±0.0005	0.2509±0.0005	0.228±0.0005	0.231±0.0005
Mean grain diameter (μm)	4.65±0.93	4.87±0.97	2.41±0.48	2.58±0.52
Unit cell dimensions (Å):				
A-axis length	3.836±0.002	3.833±0.001	3.850±0.007	3.847±0.010
B-axis length	3.887±0.001	3.886±0.001	3.889±0.006	3.889±0.007
C-axis length	11.673±0.004	11.672±0.003	11.682±0.01	11.684±0.023
Oxygen (wt%) ^a	18.2±0.18	18.0±0.18	16.4±0.66	16.8±1.60
Number of O atoms per YBCO molecule ^b	6.95±0.02	6.95±0.02	6.89±0.11	6.88±0.14

^aInert gas fusion, mean ± standard deviation for 2 trials (estimated % uncertainty = 1 % of reading).

^bCalculated (mean ± standard deviation) from ref. 20; {atoms oxygen/YBCO molecule = 76.40 - 5.95(c-axis)}; (estimated uncertainty = 0.05 atoms oxygen).

Sample A

Figure 8 shows the resulting ultrasonic velocity images constructed from the scans of sample A containing 0.10 pore fraction. A regular pattern of velocity variation of ≤ 2 percent from edge (largest velocities) to

center (lowest velocities) was observed. (The percentage change was obtained by dividing the minimum and maximum velocity values by the velocity expected for a fully-dense YBCO sample, i.e., the theoretical velocity of $0.560 \text{ cm}/\mu\text{sec}$ (ref. 21).) All images were identically reproducible within 0.1 percent.

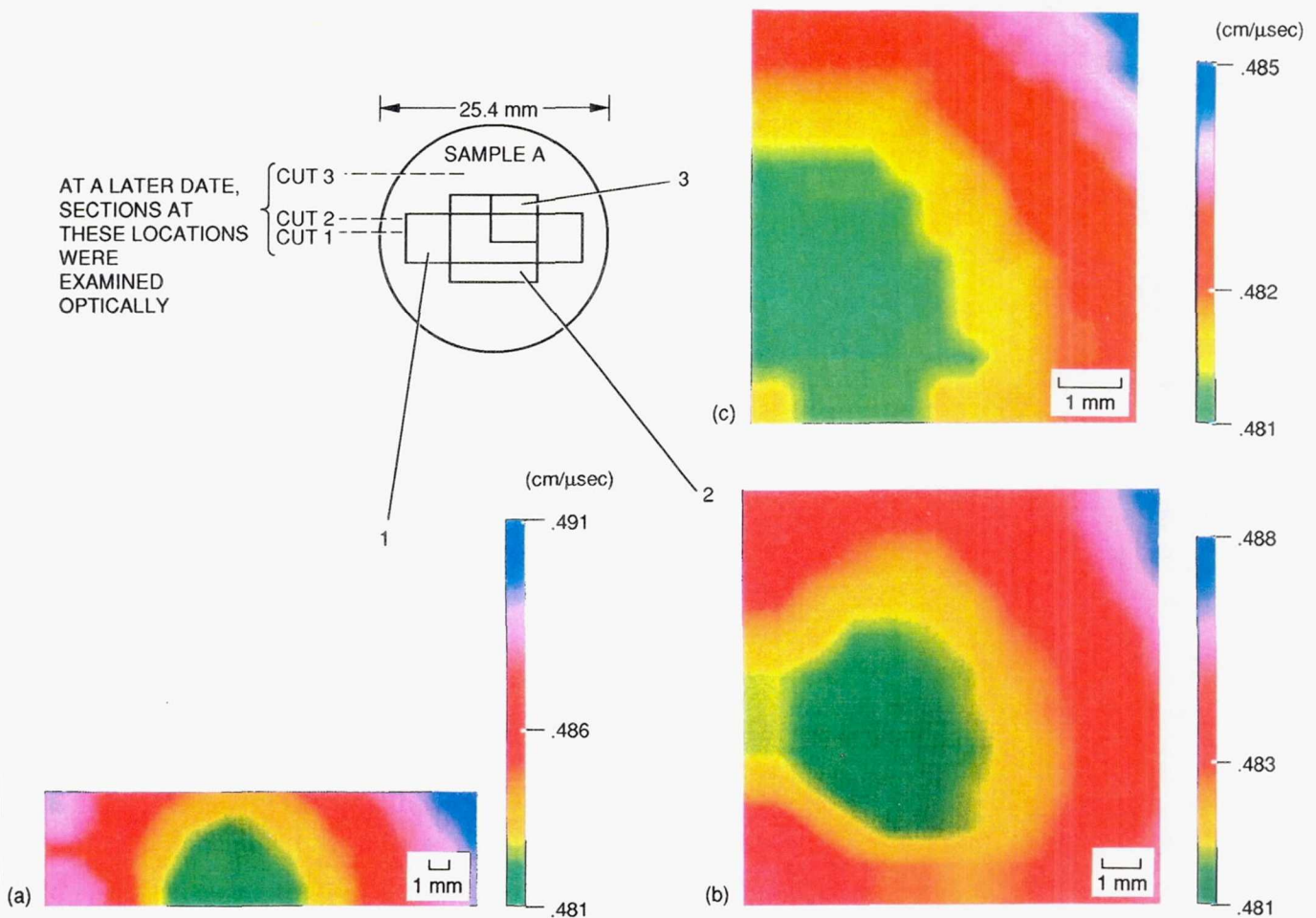


Figure 8. - Velocity images constructed from ultrasonic scans over the regions of sample A indicated. 20 MHz center frequency.

Figure 9 shows the a.c. susceptibility versus temperature responses and table II gives the superconductor properties for the edge- and center-cut bars from sample A. Markedly different behavior was observed for the bars.

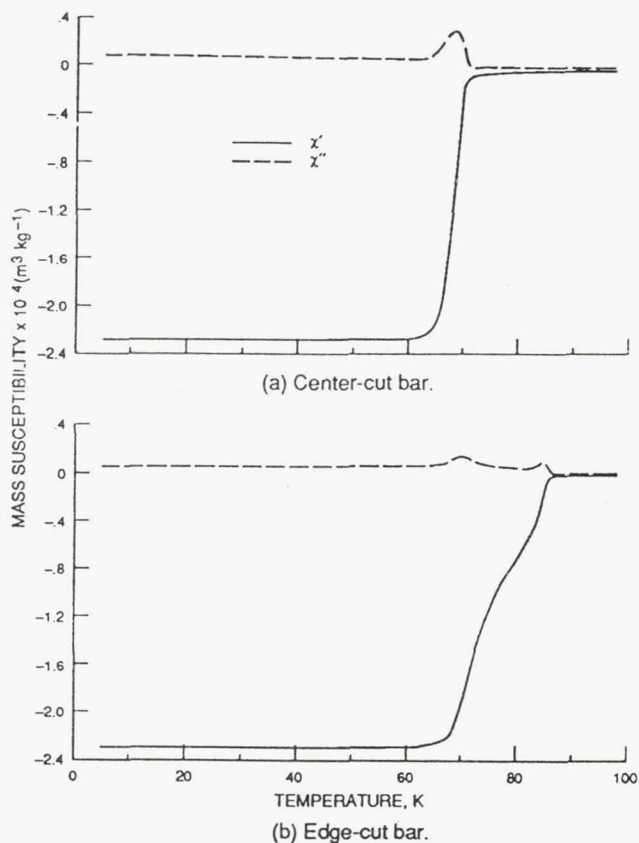


Figure 9. - A.c. susceptibility versus temperature for bars cut from sample A. $H_{ac} = 0.02 \text{ Oe}$. Frequency = 100 Hz.

For sample A, the center-cut bar exhibited a T_c of 75 K and ΔT_{cm} of 4 K. The edge-cut bar exhibited a higher T_c of about 86 K and a broader, double-sloped ΔT_{cm} of about 16.5 K. The center-cut bar was shielding close to zero magnetic flux at 77 K while the edge-cut bar was near 40 percent of maximum shielding. A single peak was observed in the χ''_m response of the center-cut bar while dual peaks were observed in the χ''_m response of bar edge-cut bar. Similar to sample 4, the within-sample property nonuniformity seen for sample A is likely to originate from compositional and/or microstructural nonuniformity. The presence

of a multi-phase material is further indicated by dual peaks in the χ''_m response for edge-cut bar (ref. 22).

No significant differences were noted in either the unit cell parameters, grain size or oxygen content for the edge- and center-cut bars of sample A (table III). However, the optical image analysis of sample A cross sections did reveal pore fraction nonuniformity from edge to center. Figure 10 shows pore fraction versus position for the three cross-sectional cuts of sample A shown in figure 5(b). Figure 10(a) shows a significant systematic mean pore fraction variation from 0.10 at the edge to 0.15 in the center for cut 1 (0.1 mm from the midplane).

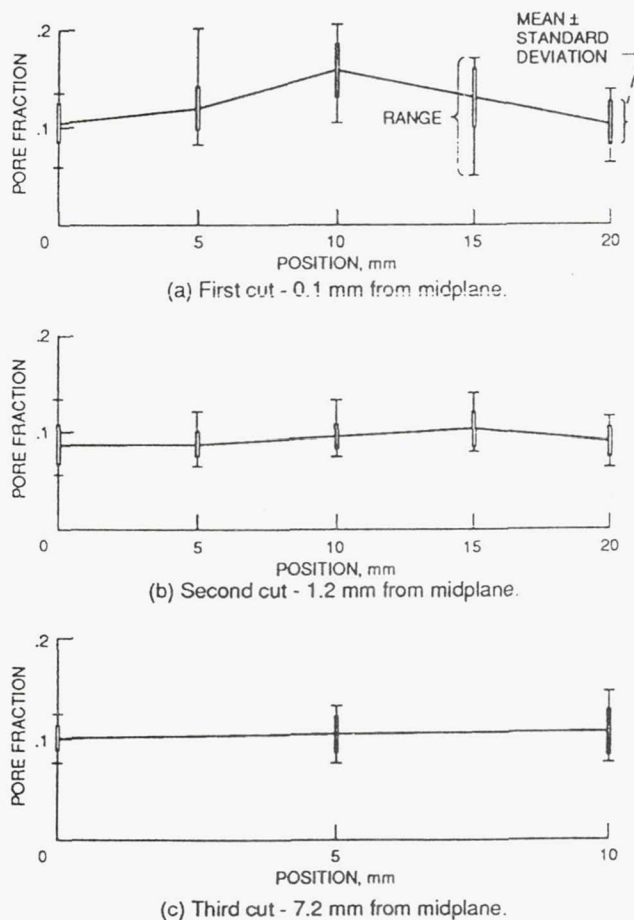


Figure 10. - Pore fraction versus position for sample A. Mean \pm standard deviation and range values for 21 fields at each position along the thickness cross-sections (means are joined).

Figures 10(b) and (c) both show an essentially uniform pore fraction of 0.09 to 0.10 for cuts 2 (1.2 mm from the midplane) and 3 (7.2 mm from the midplane). The following microstructural variables were seen not to vary along the thickness cross sections of sample A: grain size and orientation (grain size was about 2.3 μm for each of four orientations at five positions along the cross section (fig. 5(b)), CuO volume fraction (0.003 to 0.004 volume fraction of CuO was uniformly present on average from left to right edge), CuO average particle size (length and breadth were observed to be about 1 μm and 0.7 μm , respectively, irrespective of position), CuO particle orientation (appeared random from image analysis and optical micrographs), average pore size (length and breadth were observed to be about 1.8 μm and 1 μm , respectively, irregardless of position), and pore orientation (appeared random from image analysis and optical micrographs).

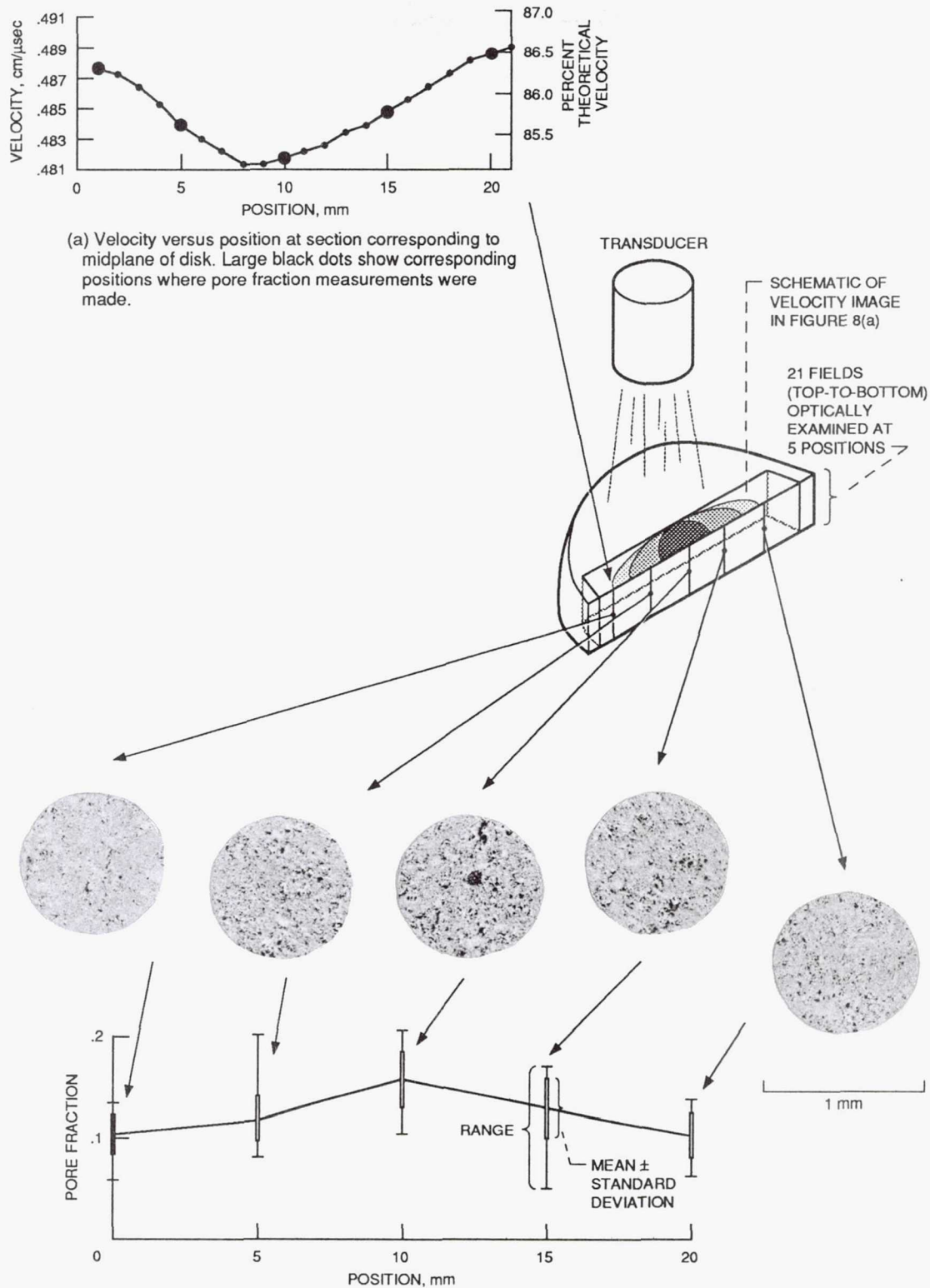
V. DISCUSSION

Correlation of Susceptibility, Microstructural and Ultrasonic Results

Oxygen content differences can result in significant differences in the a.c. susceptibility versus temperature response for YBCO (refs. 6 and 7). Since pore fraction and type (interconnected versus closed) are important factors in determining oxygen transport and hence the oxygen content in YBCO samples, (ref. 23) a correlation between pore fraction variations (fig. 10(a)) and differences in susceptibility response (fig. 9) is plausible. At high pore fractions (approximately ≥ 0.10) for YBCO samples, porosity is interconnected allowing rapid oxygenation of the sample through gas diffusion paths (ref. 23). At pore fractions of about 0.10 and below, pores close and become isolated such that pore interconnection is lessened

or eliminated. This causes oxygenation to occur by relatively slow bulk diffusion, and a much greater annealing time is required to achieve complete oxygenation. Hence, samples containing a nominal pore fraction of about 0.10 or less (such as samples 4 and A) are prone to oxygen content (and thus superconductor property) inhomogeneity since some pores may form an interconnected network while others are closed and isolated. Although inert gas fusion and x-ray diffraction analysis on the edge- and center-cut bars for sample A (and sample 4) did not indicate significant oxygen content inhomogeneity, it is possible that local oxygen content variations on a scale smaller than those tested for did exist due to the observed pore fraction variations. Macrocracking, possibly resulting from oxygenation-induced stresses present between an incompletely-oxygenated bulk and fully-oxygenated surface (ref. 7), was observed on the surface of sample 4 before cutting and machining procedures.

Pore fraction was the only microstructural variable that exhibited significant, systematic variation in sample A. This pore fraction variation occurred in cut 1 and ranged on average from 0.10 (edge) to 0.15 (center). Concerning cut 1, higher velocity corresponded to lower pore fraction at the sample edges and lower velocity corresponded to higher pore fraction at the sample center (fig. 11). This is consistent with a previous result (fig. 12) which shows a strong linear correlation between pore fraction and ultrasonic velocity for a set of YBCO specimens obtained from one manufacturer (ref. 21). For cut 3, the uniform pore fraction seen from edge to center (fig. 10(c)) agrees with the nearly uniform velocity seen across the top of the velocity image shown in figure 8(b). These results indicate that the velocity variations in sample A are likely to have resulted from pore fraction variations. This agrees with references 15 and 24 that indicate pore



(b) Pore fraction versus position. Black spots in photomicrographs indicate pores.

Figure 11. - Correlation of pore fraction and ultrasonic velocity results for sample A.

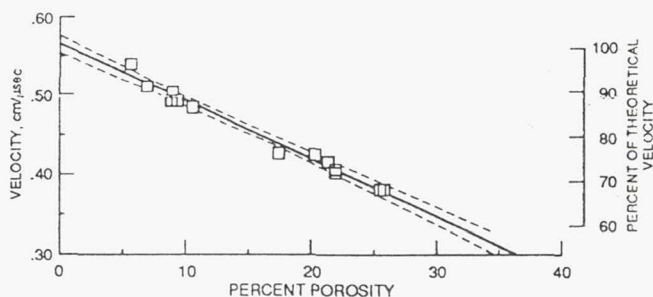


Figure 12. - Longitudinal velocity versus percent porosity for $\text{YBa}_2\text{Cu}_3\text{O}_{7-x}$ (ref. 21). Velocity = $-0.007 \times \text{percent porosity} + 0.565$. (Solid line). Percent of theoretical velocity = $-1.28 \times \text{percent porosity} + 100$. Correlation coefficient = -0.991 . Dashed lines show 95% confidence interval for mean predicted velocity values.

fraction variations are responsible for velocity variations seen in sintered SiC.

A correlation exists between susceptibility, microstructural, and ultrasonic results for sample A. It appears then that the potential exists for using ultrasonic velocity imaging to determine pore fraction variations and thus reveal potential superconductor behavior inhomogeneity in YBCO samples containing nominal pore fraction of about 0.10 or less.

A.C. Susceptibility for Samples 4 and A

While the above discussion presents an explanation for the observed susceptibility variations within samples 4 and A, it does not account for the "reverse" behavior exhibited by the edge- and center-cut bars for these samples (table II and figs. 7 and 9). For sample 4, the center-cut bar exhibited higher T_c and broader ΔT_c than did the edge-cut bar whereas the reverse was true for sample A. Microstructural and compositional analyses of samples 4 and A were not able to yield a conclusive explanation for this inhomogeneity reversal. X-ray diffraction on the starting powder for sample A indicated possible trace amounts of CuO while the starting powder for sample 4 was indicated to be phase pure.

The fact that sample A had as low a pore fraction as did sample 4 even though it was sintered at a much lower peak temperature (942°C versus 966°C) also suggested some impurity phase present in sample A during sintering (ref. 7). However, inert gas fusion analysis on the sintered samples indicated greater oxygen content (and thus the possibility of an oxide impurity phase) for sample 4. Optical image analysis indicated similar levels of CuO in both samples. Therefore, the cause of the different behavior of samples 4 and A could not be determined. It is likely that the subtle effects of starting powder condition or processing history that are difficult to measure caused the difference in superconducting behavior of samples 4 and A. The ramifications of this are that seemingly identical sample preparation procedures can produce very different results.

Quantifying Pore Fraction Variations with Ultrasonic Velocity Imaging

Based on the velocity images shown in figure 8, systematic pore fraction variations similar to those seen for cut 1 might have been expected for cut 2 since cut 2 was only about 1 mm away from cut 1 (figs. 5 and 10). This illustrates the difficulty involved in absolutely correlating between ultrasonic image results and microstructural results. The ultrasonic image represents averaged microstructural information in the volume of sample probed. Theoretically, for correlation, all two-dimensional thickness cross sections would have to be examined and the microstructural and compositional variables quantified and averaged at each plane. Additionally, uncertainty exists in the location and width of the ultrasonic beam used to approximate the volume of sample probed (ref. 19).

From reference 21 (fig. 12), it was determined that a 1 percent increase in percent porosity (%P) resulted in about a 1.3 percent

decrease in percent of theoretical velocity (%TV) for YBCO. Considering just the pore fraction results from cut 1 in sample A, a 5 percent increase in %P was apparent corresponding to a 1.5 to 2 percent decrease in %TV from edge to center. About a 6 to 7 percent decrease in %TV would have been expected. The discrepancy can be explained by noting once again that the average pore fraction in the entire volume of sample probed should be considered, not just the pore fraction in one two-dimensional plane. For example, if the pore fraction results of cuts 1 and 2 are averaged, a 3 percent increase in %P corresponding to the 1.5 to 2 percent decrease in %TV results from edge to center, which is more consistent with figure 12.

Residual stresses are likely to exist in YBCO (ref. 25) but their variation and resulting effect on velocity were not considered in this investigation. Velocity changes on the order of only 0.15 percent (steel) (ref. 26) and 0.025 percent (aluminum) (ref. 27) have been measured for metallic specimens stressed up to 200 MPa. A much greater 2 percent velocity variation was seen across sample A. This indicated that microstructural variations, and not residual stress variations, were dominant.

VI. CONCLUSION

Spatial variations in a.c. susceptibility and microstructure for $\text{YBa}_2\text{Cu}_3\text{O}_{7-x}$ samples were investigated. Samples containing 0.10 pore fraction exhibited significant differences in a.c. susceptibility versus temperature responses at edge and center locations. Samples containing higher (up to 0.25) pore fraction did not exhibit significant within-sample property nonuniformity. An ultrasonic velocity image constructed from measurements at 1 mm increments on a sample containing 0.10 pore fraction revealed microstructural nonuniformity. Bars cut from the sample at the low and high velocity

regions exhibited significantly different a.c. shielding and loss behavior. Thus, the velocity image revealed microstructural variations that correlated with variations in superconductor behavior. From quantitative optical image analysis of sample cross sections, pore fraction was revealed to be the varying microstructural feature.

ACKNOWLEDGEMENTS

The authors wish to thank Robert E. Miller of W.R. Grace and Company for his help in sample preparation.

APPENDIX A. A.C. SUSCEPTIBILITY AND SUPERCONDUCTORS

The complex a.c. susceptibility is used to measure a.c. flux exclusion (shielding) and loss in superconductors (refs. 13, and 28 to 32). In the limit of small applied field,

a.c. susceptibility represents (refs. 33 and 34).

$$\chi = \frac{dM}{dH_{ac}} \quad (4)$$

where χ is a.c. susceptibility, H_{ac} is the applied a.c. magnetic field strength and M is the magnetization of the sample.

The a.c. susceptibility measured in the zero-field cooled mode involves first cooling the sample to 4.2 K in zero applied field, applying the magnetic field, and then heating at a controlled rate through the superconducting-to-normal (S-N) transition. Applying an alternating magnetic field at 4.2 K causes currents to be established in the superconductor. The currents are composed of supercurrents flowing within grains plus intergranular supercurrents flowing in larger loops from grain to grain if the

grains are coupled (ref. 35). As the temperature is increased from 4.2 K, the real (χ') portion of the susceptibility essentially measures the degree of a.c. shielding as a function of temperature. At 4.2 K, supercurrents flow such that the maximum macroscopic volume of the sample is likely to be shielded from changes in an externally applied magnetic field (ref. 14). The imaginary portion (χ'') of the a.c. susceptibility is generally associated with heat generating a.c. power losses including eddy current losses, surface losses, and/or bulk-pinning losses from hysteresis of flux tube motion (refs. 30, and 35 to 39). A peak or peaks in χ'' versus temperature are characteristic of losses. Dual peaks are generally accompanied by abrupt slope changes in the χ' versus temperature response (ref. 22). A.c. susceptibility utilizing low frequencies ($f < 100$ Hz) minimizes the effects of eddy currents (refs. 29 and 37) and surface resistance, (ref. 40) and the peak(s) in χ'' are likely to be due to hysteresis (bulk pinning) effects (ref. 30). The use of low fields ($H_{ac} < 100$ mOe) allows the determination of first flux penetration into the material from the initial rise in χ'' (refs. 30 and 38). It is desirable for a superconductor to have shielding at any temperature and the superconducting transition temperature (T_c) as large as possible, and to have the transition width (ΔT_{cm}) and the loss peak width as small (sharp) as possible. The values for these properties are likely to be a function of sample homogeneity (ref. 7) with the most critical variable probably oxygen content (refs. 5 to 7).

APPENDIX B. ULTRASONIC VELOCITY AND MATERIAL CHANGE

In recent years, nondestructive evaluation (NDE) methods for the determination of global microstructural state have been developed to address the needs of the structural materials design community (refs. 15, 24, and 41

to 44). Ultrasonic velocity scan techniques have been shown to be useful for determining differences in the microstructural condition (strain state) from region to region within a solid (refs. 15, 24, 26, 43, 45 and 46)

When there are no boundary effects present, the velocity (V) of a longitudinal elastic wave in a bulk solid is determined by the elastic modulus (E), density (ρ), and Poisson's ratio (ν) of the solid according to (ref. 47).

$$V = \left[\frac{E(1 - \nu)}{\rho(1 + \nu)(1 - 2\nu)} \right]^{1/2} \quad (5)$$

The introduction of pores, for example, into a solid does not change modulus for the solid regions of the material. However, the apparent modulus (or stiffness) of the bulk solid is reduced by the introduction of pores (ref. 48). In theory, any material change that affects the apparent E , ρ , or ν should affect the ultrasonic velocity, i.e., velocity should be sensitive to any changes in the elastic strain state (dynamic or static) of the solid (refs. 49 and 50). Additionally, velocity should be sensitive to spatial gradients and discontinuities in the elastic state of the lattice - hence its usefulness for examining within-sample uniformity.

In practice, ultrasonic velocity is an extremely sensitive measure of material change; under the best experimental conditions, it is estimated that velocity differences on the order of 0.00001 percent can be detected (ref. 49). Changes in "monocrystal" features such as crystal structure, crystalline orientation, twin density, dislocation density, irradiation damage, charge carrier density, magnetic and electric domain wall orientation and motion, vacancy quantity, and interstitial and substitutional atom motion all have their effect in changing the velocity of high-frequency stress waves in solids (refs. 49 and 50). Changes in features normally

associated with bulk, polycrystalline materials such as pore fraction, granular, orientation, impurity concentration, residual stress, and possibly pore/impurity particle size distribution and geometry also affect velocity (ref. 21).

REFERENCES

1. J.G. Bednorz and K.A. Muller, Z. Phys. B, **64**, 189-193 (1986).
2. P.H. Hor, R.L. Meng, L. Gao, Z.J. Huang, Y.Q. Wang, K. Forster, J. Vassilio, C.W. Chu, M.K. Wu and J.R. Ashburn, Phys. Rev. Lett. **58**, 911-912 (1987).
3. H. Maeda, Y. Tanaka, M. Fukutomi, and T. Asano, Jpn. J. Appl. Phys. Lett. **27**, L209-L210 (1988).
4. Z.Z. Sheng and A.M. Hermann. Nature, **332**, 55-58 (1988).
5. R. Beyers, G. Lim, E.M. Engler, V.Y. Lee, M.L. Ramirez, R.J. Savoy, R.D. Jacowitz, T.M. Shaw, S. Laplaca, and R. Boehme, Appl. Phys. Lett. **51**, 614-616 (1987).
6. R. Beyers, B.T. Ahn, G. Gorman, V.Y. Lee, S.S.P. Parkin, M.L. Ramirez, K.P. Roche, J.E. Vazquez, T.M. Gur, and R.A. Huggins, in High Temperature Superconductors, edited by J.D. Jorgensen, Et al., (Materials Research Society, Pittsburgh, 1989), pp. 77-82.
7. D.R. Clarke, T.M. Shaw, and D. Dimos, J. Amer. Ceram. Soc. **72**, 1103-1113 (1989).
8. D.J. Roth, Property and Microstructural Nonuniformity in the Yttrium-Barium-Copper-Oxide Superconductor Determined from Electrical, Magnetic, and Ultrasonic Measurements. Ph.D. Thesis, Case Western Reserve University, 1991. (Also, NASA TM-103732.)
9. W.D. Kingery, H.K. Bowen, and D.R. Uhlmann, 1976. Introduction To Ceramics. 2nd ed., (John Wiley & Sons, New York, 1976), pp. 9 and 461-466.
10. J.W. McCauley, in Nondestructive Testing of High-Performance Ceramics, edited by A. Vary and J. Snyder, (American Ceramic Society, Westerville, OH, 1987), pp. 1-18.
11. J.E. Evetts, IEEE Trans. Magnetics, **MAG - 19**, 1109-1119 (1983).
12. R.A. Camps, J.E. Evetts, B.A. Glowacki, S.B. Newcomb, R.E. Somekh, and W.M. Stobbs, Nature, **329**, 229-232 (1987).
13. M. Couach, A.F. Khoder, and F. Monnier, Cryogenics, **25**, 695-699 (1985).
14. B.D. Cullity, Introduction to Magnetic Materials, (Addison - Wesley, New York, 1972), 1-24.
15. E.R. Generazio, D.J. Roth, and G.Y. Baaklini, Mater. Eval. **46**, 1338-1343 (1988).
16. M.A. Breazeale, J.H. Contrell Jr., and J.S. Heymann, in Methods of Experimental Physics, Ultrasonics, Vol. 19. edited by P.D. Edmonds, (Academic Press, New York, 1981), pp. 67-135.
17. D.R. Hull, H.E. Kautz, H.E., and A. Vary, Mater. Eval. **43**, 1455-1460 (1985).
18. J. Krautkramer and H. Krautkramer, Ultrasonic Testing of Materials. 2nd ed., (Springer-Verlag, New York, 1977), pp. 63-75.
19. B.M. Lempriere, in 1989 JANNAF Non-destructive Evaluation. Subcommittee Meeting, edited by M.J. Paul, CPIA-PUBL-514 (Chemical Propulsion Information Agency, Laurel, MD, 1989), pp. 115-123.

20. T. Wolf, I. Apfelstedt, W. Goldacker, H. Kupfer, and R. Flukiger, *Physica C.*, **153-155**, 351-352 (1988).
21. D.J. Roth, D.B. Stang, S.M. Swickard, and M.R. DeGuire. Review and Statistical Analysis of The Ultrasonic Velocity Method for Estimating the Porosity Fraction in Polycrystalline Materials. NASA TM-102501-REV, (1990).
22. R.B. Goldfarb, A.F. Clark, and A.I. Branginski, *Cryogenics*, **27**, 475-480 (1987).
23. N. McN. Alford, W.J. Clegg, M.A. Harmer, J.D. Birchall, K. Kendall, and D.H. Jones. *Nature*, **332**, 58-59 (1988).
24. D.C. Kunnerth, K.L. Telschow, and J.B. Walter, *Mater. Eval.* **47**, 571-575 (1989).
25. E.A. Fisher, in Proceedings of the Workshop on Nondestructive Evaluation of Residual Stress, NTIAC-76-72, (National Testing Information Analysis Center, San Antonio, TX, 1975), pp. 125-126.
26. J.C. Shyne, N. Grayelli, and G.S. Kino, Nondestructive Evaluation. edited by O. Buck and S.M. Wolf, (Metallurgical Society of AIME, Warrendale, PA, 1981) pp. 133-146.
27. A. Zeiger and K. Jassby, *J. Non-destructive Eval.*, **3**, 115-124 (1982).
28. M. Davis, S. Wolf, R. Soulen, and W. Fuller, Report on DARPA Round Robin. 1989. DARPA High Temperature Superconductor Measurements Workshop. Apr. 17-18, 1989, Washington, D.C.
29. R.A. Hein, H. Hojani, A. Barkatt, H. Shafii, K.A. Michael, A.N. Thorpe, M.F. Ware, and S. Alterescu, *J. Superconductivity*, **2**, 427-461 (1989).
30. R.B. Goldfarb, A.F. Clark, A.J. Panson, and A.I. Braginski, in High Temperature Superconductors. edited by D.U. Gubser and M. Schluter, (Materials Research Society, Pittsburgh, 1987) pp. 261-263.
31. R.A. Hein, *Phys. Rev. B*, **33**, 7539-7549 (1986).
32. H. Kupfer, I. Apfelstedt, R. Flukiger, C. Keller, R. Meier-Hirmer, B. Runtzsch, A. Turowski, U. Weich, and T. Wolf, *Cryogenics*, **28**, 650-660 (1988).
33. A.J.V. Duyneveltdt, AC - Susceptibility Studies in Solid State Magnetism. *Proc. Letnia Szkola Magnetyzmu, Bialowieza*, pp. 1-39.
34. R.B. Goldfarb, *Cryogenics*, **26**, 621-622 (1986).
35. H. Dersch and G. Blatter, *Phys. Rev. B*, **38**, 11391-11404 (1988).
36. B. Barbara, A.F. Khoder, M. Couach, and J.Y. Henry, *Europhys. Lett.*, **6**, 621-627 (1988).
37. D.X. Chen, J. Nogues, and K.V. Rao, *Cryogenics*, **29**, 800-808 (1989).
38. B. Loegel, A. Mehdaoui, and D.J. Bolmont. *Less Common Metals*, **150**, 193-199 (1989).
39. A. Mehdaoui, B. Loegel, D. Bolmont, J. Baron, G. Nanse, and M. Soulard, *Sol. St. Comm.* **68**, 333-336 (1988).

40. J.D. Doss, Engineer's Guide To High-Temperature Superconductivity. John Wiley & Sons, New York, 1989) pp. 81-88, 111 and 122-124.
41. W.A. Sanders and G.Y. Baaklini, *Adv. Ceram. Mater.*, 3, 88-94 (1988).
42. W.A. Ellingson, W.S. Wong, S.L. Dieckman, J.L. Ackerman, and L. Garrido. *Am. Ceram. Soc. Bull.*, 68, 1180-1186 (1989).
43. J.J. Gruber, J.M. Smith, and R.H. Brockelman, *Mater. Eval.*, 46, 90-96 (1988).
44. C.S. Vikram and C.O. Ruud, in Review of Progress in Quantitative Nondestructive Evaluation, Vol. 5B. edited by D.O. Thompson and D.E. Chimenti, (Plenum Press, New York, 1986), pp. 1327-1334.
45. N.N. Hsu, T.M. Proctor Jr., and G.V. Blessing, *Test. and Eval.*, 10, 230-234 (1982).
46. G.S. Kino, D.M. Barnett, N. Grayelli, G. Herrman, J.B. Hunter, D.B. Ilic, G.C. Johnson, R.B. King, M.P. Scott, and J.C. Shyne, *J. Nondestructive Eval.*, 1, 67-77 (1980).
47. J. Szilard, in Ultrasonic Testing. edited by J. Szilard, (Wiley, New York, 1982), pp. 1-23, 217-261.
48. R.W. Rice, in Properties of Microstructure: Treatise on Materials Science and Technology, Vol. 11. edited by R.K. MacCrone, (Academic Press, New York, 1977), pp. 199-381.
49. G.A. Alers, Physical Acoustics, Vol. IV, Part A. edited by W.P. Mason, (Academic Press, New York, 1966) pp. 277-297.
50. R. Truett, C. Elbaum, and B.B. Chick, in Ultrasonic Methods in Solid State Physics, (Academic Press, New York, 1969), pp. 77-78 and 159-179.



National Aeronautics and
Space Administration

Report Documentation Page

1. Report No. NASA TM - 103787	2. Government Accession No.	3. Recipient's Catalog No.	
4. Title and Subtitle Spatial Variations in A.C. Susceptibility and Microstructure for the $\text{YBa}_2\text{Cu}_3\text{O}_{7-x}$ Superconductor and Their Correlation with Room- Temperature Ultrasonic Measurements		5. Report Date	
		6. Performing Organization Code	
7. Author(s) Don J. Roth, Mark R. DeGuire, Leonard E. Dolhert, and Aloysius F. Hepp		8. Performing Organization Report No. E - 6064	
		10. Work Unit No. 506 - 43 - 11	
9. Performing Organization Name and Address National Aeronautics and Space Administration Lewis Research Center Cleveland, Ohio 44135 - 3191		11. Contract or Grant No.	
		13. Type of Report and Period Covered Technical Memorandum	
12. Sponsoring Agency Name and Address National Aeronautics and Space Administration Washington, D.C. 20546 - 0001		14. Sponsoring Agency Code	
15. Supplementary Notes Prepared for the 93rd Annual Meeting of the American Ceramic Society, Cincinnati, Ohio, April 28 - May 2, 1991. Don J. Roth, NASA Lewis Research Center; Mark R. DeGuire, Case Western Reserve University, Cleveland, Ohio 44106; Leonard E. Dolhert, W.R. Grace & Company, Columbia, Maryland 21044. Aloysius A. Hepp, NASA Lewis Research Center. Responsible person, Don J. Roth, (216) 433 - 6017.			
16. Abstract The purpose of this study was to 1) examine the spatial (within-sample) uniformity of superconducting behavior and microstructure in $\text{YBa}_2\text{Cu}_3\text{O}_{7-x}$ specimens over the pore fraction range 0.10 - 0.25 and 2) determine the viability of using a room-temperature, nondestructive characterization method (ultrasonic velocity imaging) to predict spatial variability. Spatial variations in superconductor properties were observed for specimens containing 0.10 pore fraction. An ultrasonic velocity image constructed from measurements at 1 mm increments across one such specimen revealed microstructural variation between edge and center locations that correlated with variations in a.c. shielding and loss behavior. Optical quantitative image analysis on sample cross-sections revealed pore fraction to be the varying microstructural feature.			
17. Key Words (Suggested by Author(s)) Superconductors; Ceramics; Ultrasonics; Velocity; A.C. susceptibility; Spatial variations; Microstructure; Yttrium-barium-copper-oxide; Nondestructive evaluation		18. Distribution Statement Unclassified - Unlimited Subject Category 38	
19. Security Classif. (of the report) Unclassified	20. Security Classif. (of this page) Unclassified	21. No. of pages 22	22. Price* A03